J. Fluid Mech. (1975), *vol.* 70, *part* 3, *pp.* 417–436
Printed in Great Britain

Wind-generated gravity–capillary waves: laboratory measurements of temporal growth rates using microwave backscatter

By T. R. LARSON† AND J. W. WRIGHT
Ocean Sciences Division, Naval Research Laboratory, Washington, D.C. 20375

(Received 22 March 1974)

The growth rates of wind-induced water waves at fixed fetch were measured in a laboratory wave tank using microwave backscatter. The technique strongly filters out all wavenumber component pairs except for a narrow window at the resonant Bragg scattering conditions. For these waves the spectral amplitude was measured as a function of the time after a fixed wind was abruptly started. The radars were aligned to respond to waves travelling in the downwind direction at wavelengths of 0·7–7 cm. Wind speeds ranged from 0·5 to 15 m/s. Fetches of 1·0, 3·0 and 8·4 m were used. In every case, the spectral amplitude initially grew at a single exponential rate β over several orders of magnitude, and then abruptly ceased growing. No dependence of the growth rate on fetch was observed. For all wavelengths and wind speeds the data can be fitted by

$$\beta(k, u_*, \text{fetch}) = f(k)\, u_*^n,$$

with $n = 1{\cdot}484 \pm 0{\cdot}027$. Here u_* is the friction velocity obtained from vertical profiles of mean horizontal velocity. For each wind speed, $f(k)$ had a relative maximum near $k = k_{\min} \simeq 3{\cdot}6\,\text{cm}^{-1}$. Rough estimates of $\beta/2\omega$, where ω is the water wave frequency, and of the wind stress supported by short waves indicate that the observed growth rates are qualitatively very large. These waves are tightly coupled to the wind, and play a significant role in the transfer of momentum from wind to water.

1. Introduction

Wind blowing over an air–water interface produces surface waves. The interactions between wind and waves, and among waves, have been the subject of several experimental studies (Gottifredi & Jameson 1970; Hidy & Plate 1966; Hsu & Yu 1970; Lai & Shemdin 1969; Stewart 1970; Sutherland 1968; Wilson *et al.* 1973). Although it is highly plausible that short surface waves grow as the result of linear instability of the mean shear flow near the air–water interface it has not been possible to obtain quantitative agreement between theory and experiment (Stewart 1970; Wilson *et al.* 1973). The work reported here extends the study of wave growth rates into heretofore inaccessible ranges of wind speed and water

† Present address: Ball Brothers Research Corp., P.O. Box 1062, Boulder, Colorado 80303.

wavelength, using microwave scattering as the probing technique. This technique is described in §2. The results reported here are measurements of the initial temporal growth of waves when a wind is abruptly started over a calm water surface. The transient properties of this wind field are discussed in §3 and the steady-state properties in appendix A. The water wave amplitude is small in the initial stages of growth. Hence the microwave scattering is of first order in the surface displacement, so that a single water wavelength is selected for study by the first-order Bragg scattering condition (§2, equation (5)).

The temporal-growth technique is generally more appropriate for measurements of the growth of short waves than the conventional technique of measuring the variation of wave amplitude with fetch. To see this, consider the evolution of the power spectrum $\Psi(k, x, t)$ of surface displacements with fetch x and time t as described by a transport equation (Hasselmann 1968)

$$c_g(k)\frac{\partial \Psi(k)}{\partial x} + \frac{\partial \Psi(k)}{\partial t} = \beta_m(k)\,\Psi(k) + I(k). \tag{1}$$

Here $\beta_m(k)$ is the wind-induced growth rate to be measured, $I(k)$ is a functional describing wave–wave interactions (for the second-order conservative interactions among short waves see Valenzuela & Laing 1972) and

$$c_g(k) = \partial\omega/\partial k. \tag{2}$$

For the short-wavelength waves (7–0·7 cm) considered here growth is limited by the interactions, i.e. in the steady state

$$\beta_m(k)\,\Psi(k) + I(k) \simeq 0, \tag{3}$$

so that

$$|\beta_m(k)|\,\Psi(k)| \simeq |I(k)| \gg |c_g(k)\,\partial\Psi(k)/\partial x|. \tag{4}$$

Thus measurements of $\partial\Psi/\partial x$ in the steady state may not give direct information about β_m. In the initial stages of temporal growth, however, the resonant interactions are negligible and the initial growth rate can yield β_m directly. Microwave scattering is well suited to transient measurements because spatial averaging over the surface area illuminated by the antenna (several water wavelengths per side in these measurements) is inherent. This substantially reduces the number of growth curves which must be measured to obtain reproducible values for the growth rate. Measured values of initial growth rates are presented and discussed in §4.

2. Wave probe and tank

The microwave techniques used in this study are described by Wright (1966), Wright & Keller (1971) and Duncan, Keller & Wright (1974). A unique feature is the use of focused parabolic antennae to obtain an effectively plane electromagnetic wave in the near field of the antennae and to control the illuminated water surface area. For depression angles θ (see figure 1) away from 90° the dominant scattering mechanism is Bragg scattering even in the steady state (Wright & Keller 1971). In the initial growth stage studied in this experiment the wave amplitude is much smaller and the applicability of first-order scattering

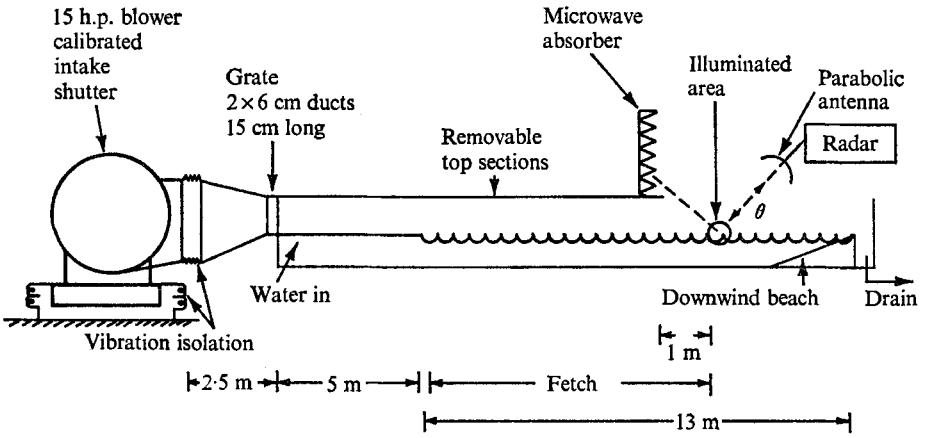

FIGURE 1. Sketch (not to scale) of the wind-wave facility used for these growth measurements. Wind-tunnel height = 30 cm, water depth = 30 cm, tank width = 1·2 m. Fetches used: 1·0, 3·0 and 8·4 m.

λ_B (cm)	k_B (cm^{-1})	θ (deg)	f_0 (GHz)	f_i (Hz)
6·98	0·90	60	4·283	4·85
4·05	1·55	30	4·283	6·76
2·72	2·31	54	9·375	9·00
1·85	3·40	30	9·375	12·7
1·25	5·01	60	23·9	19·1
0·72	8·67	30	23·9	38·1

TABLE 1

theory unequivocal. In that case the backscattered power is proportional to $\Psi(\mathbf{k}_B)$, where $\mathbf{k}_B$ is the Bragg wave vector. For backscatter the Bragg wave vector $\mathbf{k}_B = (k_x, k_y)$ is defined by

$$\left.\begin{aligned} k_y &= 0, \\ k_x &= 2k_0 \cos\theta \equiv k_B, \\ \text{or} \qquad \lambda_B &= \lambda_0/(2\cos\theta), \end{aligned}\right\} \tag{5}$$

where k_0 and λ_0 are the incident microwave wavenumber and wavelength respectively. The values of λ_0 and θ for the six Bragg wavelengths studied are given in table 1. The proportionality between backscattered power and mean-square wave height in first-order scattering is essentially one of definition (Wright 1968), but see Wright (1966) for an experimental verification. The antenna pattern at the water surface (both phase and amplitude) determines the resolution in wavenumber. In the case of horn antennae it is possible to make a qualitatively correct calculation of the antenna function determining this resolution (Wright & Keller 1971) but in the case of focused parabolas it is simpler to measure it using monochromatic, mechanically generated waves as outlined by Duncan *et al.* (1974). Let Δk be the half-width of the antenna response

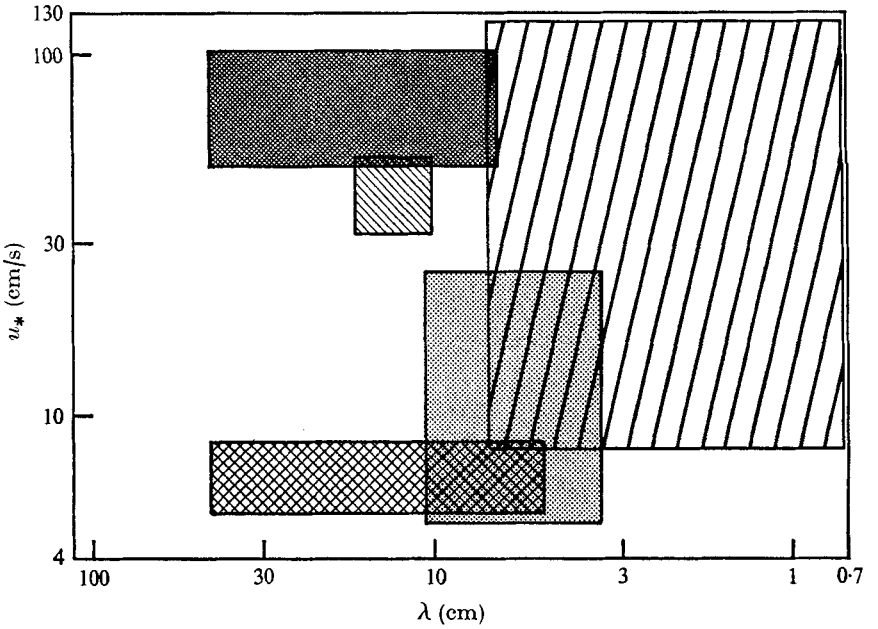

FIGURE 2. Ranges of independent variables, wind speed and water wavelength, studied in this work and in the four previous growth studies. Note the logarithmic scales. ⁞⁞⁞, Gottfredi & Jameson; ▨, Wilson *et al.*; ▥, Hidy & Plate; ▩, Sutherland; ////, this work.

at the level 6 dB below the peak response. The resolution $\Delta k_x/k_B$ in the upwind–downwind direction varied from 10 % for the 4·3 GHz (7 cm) antenna to less than 3 % for the 23·96 GHz antenna. In the orthogonal direction, Δk_y was less than 0·2 cm^{-1}.

Since the scatterers are waves and the waves are moving, the backscattered power is Doppler shifted. In first-order scattering (5) this Doppler shift is identically the frequency of the scattering wave in the laboratory frame independent of the dispersion relation. Contributions to the phase speed of the Bragg wave in the laboratory frame may come from the mean wind drift and the orbital velocity of larger waves. The effect of the wind drift on the phase speed in the steady state is discussed by Keller, Larson & Wright (1974). Since longer waves grow more slowly, advection of the Bragg wave by the longer waves should be negligible in the initial stages of Bragg wave growth. The existence of a Doppler shift in the backscattered power has the important practical consequence that unshifted reflexions from stationary objects in the room can be discriminated against by filtering. The minimum detectable wave height was limited, in practice by how well these unwanted reflexions could be filtered out, and nulled out, by balancing a microwave bridge. Water wave amplitudes of less than 10 μm were readily measurable. The dynamic range of the microwave system exceeds 100 dB in received power when transmitting one watt. The actual linear dynamic range was limited by the audio frequency circuitry discussed in §3.

The wind–wave facility used is sketched (not to scale) in figure 1, where important dimensions are given. A shutter on the constant-speed centrifugal

blower could be abruptly opened to a pre-set final value. The tank was covered down to the working fetches of 1·0, 3·0 or 8·4 m except for the last 1·0 m, which was left uncovered to facilitate the microwave measurements. Profiles of mean air velocity as a function of vertical position were measured for various wind speeds and at several positions. A detailed discussion of the steady-state airflow properties of the tank is given in appendix A. The maximum wind speed was 15 m/s, corresponding to a friction velocity u_* of 124 cm/s. (Friction velocity is defined in appendix A.) The ranges of wind speed and wavelength used in this study are indicated in figure 2, together with those of previous workers. Note that microwave scattering allows us to study wind speeds an order of magnitude higher and wavelengths an order of magnitude shorter. Several precautions were taken to prevent surface films of contaminant. These are described in appendix B together with measurements of the damping of mechanical waves which were made to check surface cleanliness.

3. Measurement of wave growth in a transient wind field

As was previously pointed out, for the small wave amplitudes in the initial stages of temporal growth the backscattered power is proportional to $\Psi(\mathbf{k}_B)$ and the growth of both the spectrum and backscattered power is expected to be exponential. We found that this was indeed the case provided that we averaged the growth curves properly. In discussing the averaging procedure we must first point out that the microwave detection scheme used (e.g. Wright 1966) results in a receiver output voltage $V_0(t)$ which is proportional to the modulus of the instantaneous received microwave field, i.e. to the square root of the instantaneous received power. This voltage was filtered using a band-pass filter with a flat response between 1 and 100 Hz. This discriminated against unwanted room reflexions which appear at d.c. and high frequency noise components. The best procedure at this point would have been to generate the r.m.s. value of $V_0(t)$. Unfortunately we did not have an analog r.m.s. device of sufficient linear dynamic range. Thus the procedure actually used was to take the absolute value of $V_0(t)$ and average. For processes of narrow bandwidth this procedure yields a result differing by a constant factor from that of the optimum processing. The fractional bandwidth $\beta_m(k_B)/\omega_B$ in the initial growth stages, where ω_B is the angular frequency of the Bragg wave, had a maximum value of 0·2 as will be seen. Furthermore the measured quantity, the growth rate, is amplitude independent. Thus we believe that the averaging procedure used is sufficiently accurate.

Two techniques were used for the averaging process referred to above. The first, used for most of the data, was to pass $|V_0(t)|$ through an analog integrator with $RC = T_i = 1{\cdot}0$ s. For an input v_1 given by

$$v_1 = V_0 \exp(\tfrac{1}{2}\beta t) \tag{6}$$

the output v_2 of such a filter is

$$v_2 = V_0 \exp(\tfrac{1}{2}\beta t)/(1 + \tfrac{1}{2}\beta T_i) \tag{7}$$

after an initial time delay

$$T_0 = (2/\beta)\ln(1 + \tfrac{1}{2}\beta T_i). \tag{8}$$

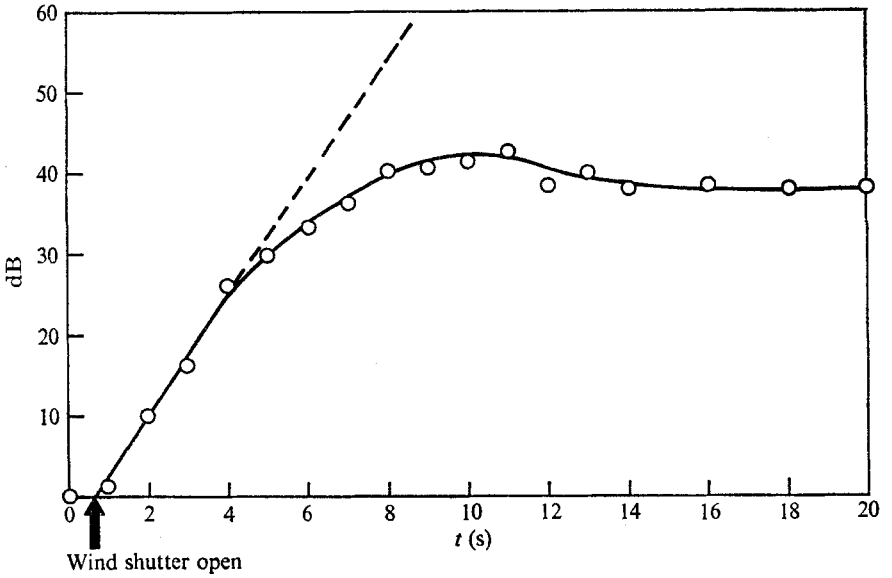

FIGURE 3. Backscattered microwave power plotted on a logarithmic scale *vs.* time. Slope gives $\beta = 1{\cdot}72\ \mathrm{s}^{-1} \pm 5\,\%$, $\lambda = 4{\cdot}05$ cm, $u_{*\mathrm{final}} = 34\ \mathrm{cm/s} \pm 5\,\%$.

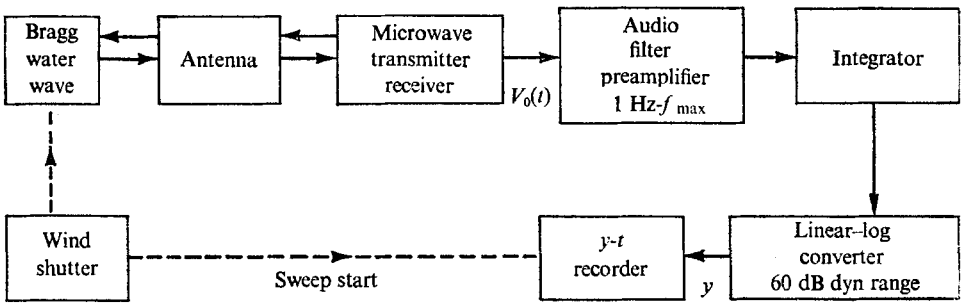

FIGURE 4. A block diagram illustrating the data processing used to measure initial growth rates.

Thus the growth rate of an exponentially growing input signal is retained. The slight initial delay and reduction in dynamic range were acceptable. For each set of experimental conditions, at least three measurements were made using this technique and the results averaged to give a measured growth rate. As a check on this procedure, a growth-rate measurement was repeated 20 times under identical conditions with $T_i = 0{\cdot}001$ s, i.e. with no averaging. These data were averaged manually (see figure 3), and yielded the same growth rate, to within 5 %, as the previous technique.

Since the exponential growth rate was of primary interest, the logarithm of the averaged signal was taken with an analog lin–log converter and plotted *vs.* time on a y–t plotter synchronized with the opening of the fan shutter. The lin–log converter had a flat frequency response from zero to at least 1 kHz and the plotter slewing speed, at the gain settings used, allowed measurement of exponential

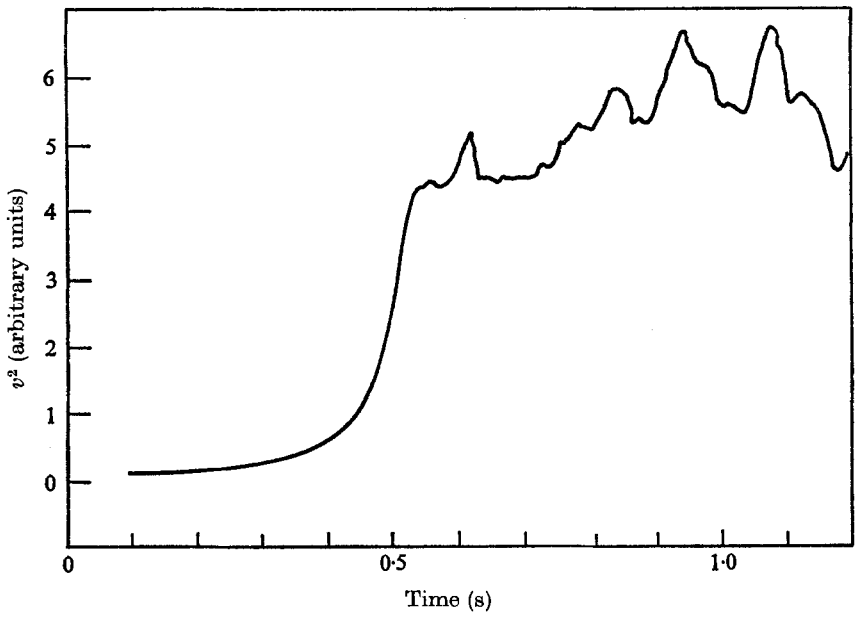

FIGURE 5. Wind transience produced by shutter opening. The trace shows the pressure transducer output of a Pitot-static tube placed at a 8·4 m fetch, 12 cm above mean water level.

$u_{*\text{final}}$ (cm/s)	Wind growth rate (s^{-1}) ($\pm 10\%$)	Wind growth time, T_α (s) ($\pm 10\%$)
124	10·6	0·40
85	7·8	0·48
46	4·6	0·68
17	2·7	0·79

TABLE 2

growth rates up to 57 s^{-1}, about 50 % greater than the maximum observed. The overall linear dynamic range of the system was 60 dB in relative backscattered power. A block diagram of the system is shown in figure 4.

The increase in wind velocity with the time after opening the shutter was monitored at the longest fetch. The same Pitot-static tube and transducer as were used for the velocity profiles was mounted at $z = 12$ cm above the calm water level, centred above the illuminated area. The wind speed grew exponentially from the initial light value, the growth slowing abruptly at a value within 10 % of the mean final wind speed. Figure 5 illustrates an oscilloscope trace of pressure transducer output voltage *vs.* time. Note that the voltage plotted is proportional to the square of the wind velocity. No significant difference in the wind growth rate was observed when a 6·4 mm diameter Pitot tube

was substituted for the 3·2 mm diameter tube. The frequency response of the pressure transducer was not a limitation.

Measured exponential wind growth rates are given in table 2 together with values of T_α, the time required for the wind speed to reach its final value. In all cases a region of exponential growth at least 4–5 times longer than T_α was observed. Thus the finite time required for the wind to reach a steady state did not hinder the determination of wave growth rates. Any region of linear (in time) wave growth at small wave amplitudes may have been obscured by the growing wind or by the averaging technique described above. In any case no region of linear growth was observed. The growth rate of the wind drift is unknown but we emphasize that in all the measurements reported here an unambiguous, single, exponential growth in backscattered power over 2–5 orders of magnitude was observed. Thus, to the extent that the transient properties of the highly sheared portions of the flow on either side of the air–water interface affect the wave growth rate, they must be considered an integral part of the process of temporal wave growth.

4. Measured wave growth rates

For every set of experimental conditions observed, the water wave of Bragg wavelength grew initially at a single exponential rate over several orders of magnitude in wave spectral amplitude. This behaviour is illustrated in figure 3, in which an average of twenty traces of relative backscattered power is plotted logarithmically *vs.* time. In each case, the shutter was opened, with the constant-speed blower running, at the time indicated. The overshoot behaviour observed and illustrated in figure 3 may be the temporal analogue of the oscillations with fetch observed by Mitsuyasu (1969).

The initial exponential growth rate was measured as a function of three independent variables: the fetch, wind speed and Bragg wavelength. As stated previously, the three working fetches were 1·0, 3·0 and 8·4 m. The wind speed range covered 1·25 decades; u_* was varied from 7 to 124 cm/s, corresponding to a $v_{\max}$ ranging from 1·4 to 15 m/s. Six water wavelengths were studied, spanning the decade from 0·7 to 7 cm. Growth rates were measured for more than eighty combinations of these three independent variables. Each measurement consists of an average of the slopes obtained from a trace of the logarithm of the returned power *vs.* time for each of at least three, and usually five, runs.

The measured growth rate β_m is the result of the superposition of all processes leading to exponential growth. In assessing the wind-speed dependence of the growth rate, however, it is a good thing to remove the portion independent of the wind speed, and due to viscous damping. Since wall damping can be neglected when the wavelengths are much less than the tank width (Wilson *et al.* 1973), we define a net growth rate β by

$$\beta_m = \beta - 4\nu k^2. \tag{9}$$

The value of the kinematic viscosity ν used was 0·011 cm^2/s (appendix B). The viscous damping correction (9) is insignificant except at light winds. The

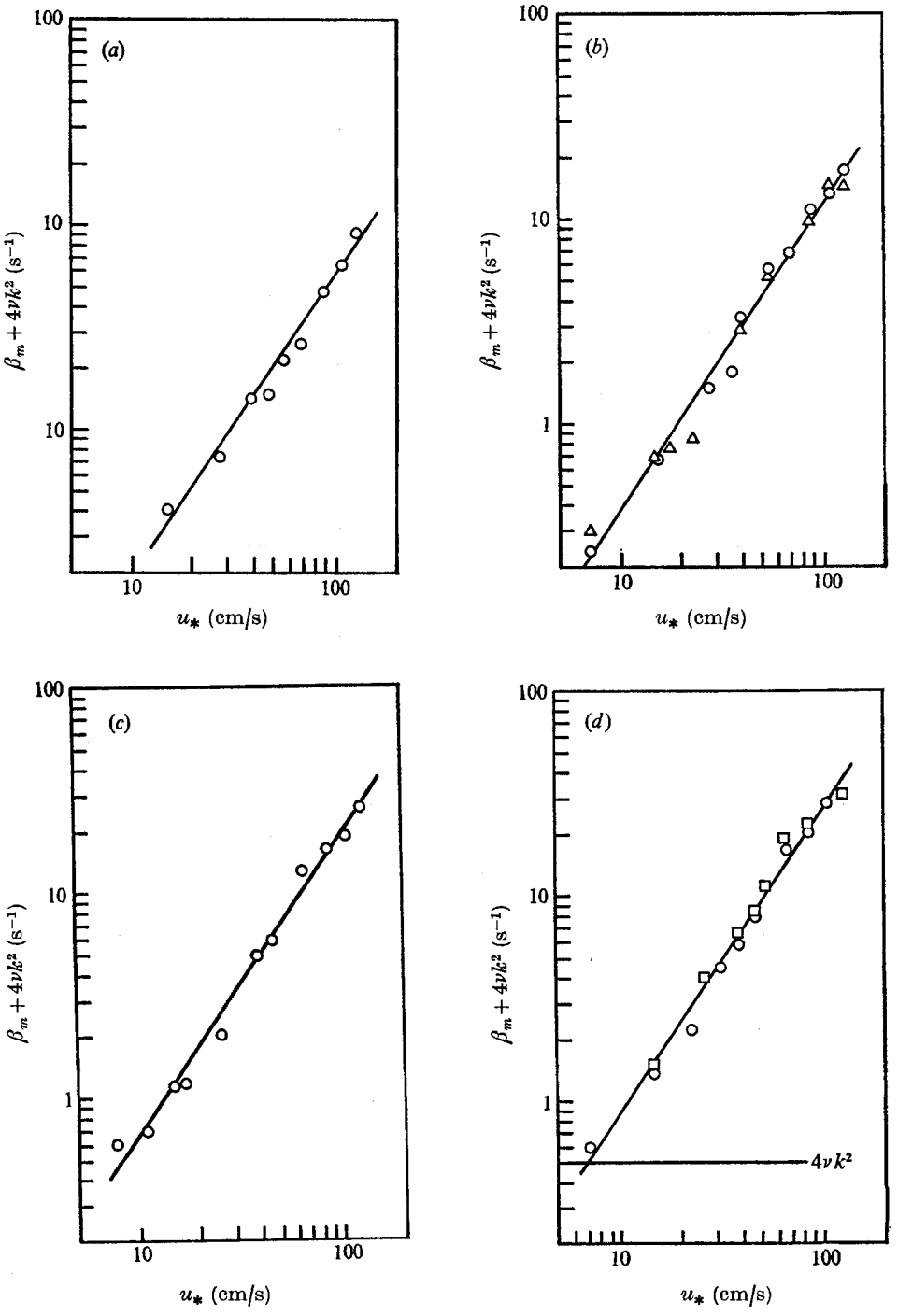

FIGURES 6 (*a–d*). For legend see next page.

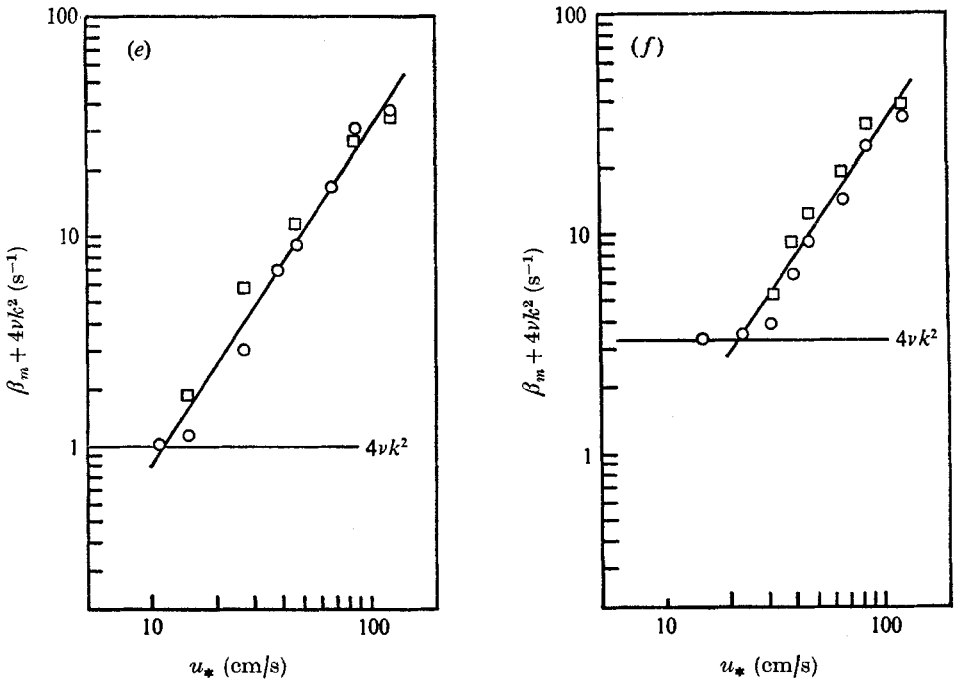

FIGURE 6. Observed growth rates *vs.* friction velocity. Fetches: □, 1·0 m; ○, 3·0 m; △, 8·4 m. (*a*) $k = 0{\cdot}90$, $\lambda = 6{\cdot}98$ cm. (*b*) $k = 1{\cdot}55$, $\lambda = 4{\cdot}05$. (*c*) $k = 2{\cdot}31$, $\lambda = 2{\cdot}72$. (*d*) $k = 3{\cdot}40$, $\lambda = 1{\cdot}85$. (*e*) $k = 5{\cdot}01$, $\lambda = 1{\cdot}25$. (*f*) $k = 8{\cdot}67$, $\lambda = 0{\cdot}72$.

condition $\beta(k_B) < 4\nu k_B^2$ was avoided for the shorter-wavelength waves because under these conditions waves of wavenumber $k < k_B$ could grow, approach a steady state and produce parasitic waves of wavenumber k_B even though no initial growth at k_B had occurred. This presented the interesting possibility of measuring interaction times for the production of parasitic waves but this was beyond the scope of this work. All growth rates reported here, including those for the largest wavenumbers, should be characteristic of freely propagating waves.

Observed net growth rates β are plotted *vs.* u_* for each of the six wavelengths in figures 6 (*a*)–(*f*). The viscous damping correction is indicated where it is visible on the scale. As can be seen from comparison of data taken at various fetches (indicated in the figures), no significant dependence of the growth rate on fetch was observed. The log–log plots in figures 6 (*a*)–(*f*) reveal a power-law dependence of β on u_*:

$$\beta \propto u_*^n. \tag{10}$$

The straight lines drawn through the data are the result of a least-squares fit assuming equally weighted data points. The resulting slopes are plotted (on an expanded vertical scale) *vs.* k in figure 7. The error bars indicate one standard deviation on either side of the plotted slope. The data are consistent with a single value of n, independent of k. The mean of these six slopes gives

$$n = 1{\cdot}484 \pm 0{\cdot}027, \tag{11}$$

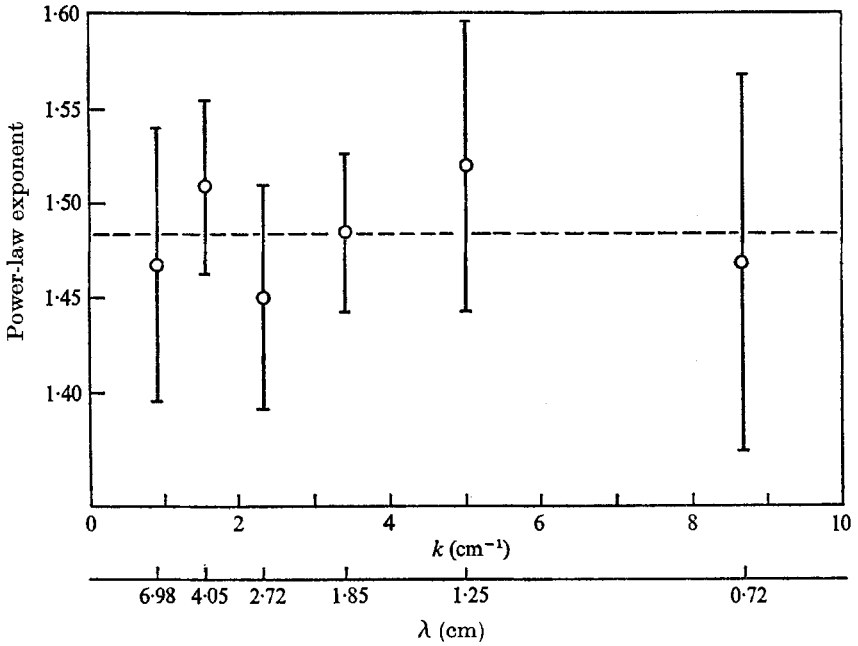

FIGURE 7. Slopes of the straight-line fits to figures 6(*a*)–(*f*) *vs.* *k*. Error bars are ± one standard deviation. Note the expanded vertical scale. $\beta \propto u_*^{1{\cdot}484 \pm 0{\cdot}027}$.

where ±0·027 is ± one standard deviation. Thus the power law given by (10) fits all of the data for three fetches, for a decade range of wavelengths, for over a decade range of wind speeds and for a total range of over two decades of β. Note that $n = \frac{3}{2}$ fits within the error bounds of (11). To indicate the overall goodness of fit, a standard deviation of individual data points relative to the fitted values was calculated for each of figures 6(*a*)–(*f*). These are given, in per cent, in the last column of table 1. The mean of the six values is 18%. The individual runs averaged to give a single value of β_m had a spread of ±10%, which is consistent with the goodness of fit given above. Several cases were repeated over a period of four to six weeks, and reproducibility was always within this ±10% spread.

A more complete functional description of the data is

$$\beta(k, u_*, \text{fetch}) = f(k)\, u_*^n. \tag{12}$$

To show the wavelength dependence, β is plotted *vs.* k in figure 8 for five representative wind speeds. The solid lines connect points determined from the straight lines fitted to the data in figure 6. The data points plotted are only those taken at the five wind speeds given. The line labelled $4\nu k^2$ indicates the viscous damping term added. A relative maximum in $\beta(k)$ is indicated for each wind speed. Note that this maximum occurs near $k_m \simeq 3{\cdot}7\ \text{cm}^{-1}$, the wavenumber of minimum phase speed for infinitesimal irrotational waves.

There are few, if any, comparable measurements of temporal wave growth for short waves. Most measurements have been of wind wave spectral development with fetch as mentioned in the introduction. However our wave growth data are

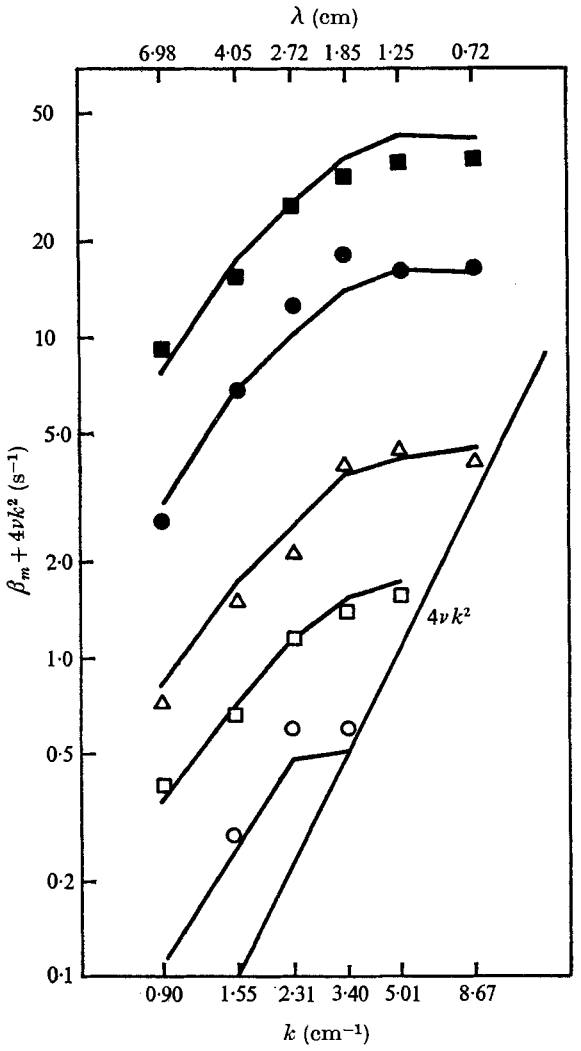

FIGURE 8. Observed growth rates β *vs.* k for five representative wind speeds. The lines connect points obtained from the fits of figures 6(*a*)–(*f*). The viscous damping correction discussed in the text is indicated ($\nu = 0{\cdot}011$ cm^2/s). u_* (cm/s): ○, 7; □, 15; △, 27; ●, 66; ■, 124.

plotted in the form β/k *vs.* k in figure 9 together with results of several other experimental studies, as indicated. Values of β in other studies were measured with point probes and were given as a function of wave frequency. These have been reduced to the form β/k *vs.* k using the dispersion relation for infinitesimal waves

$$\omega_i^2 = (980\,\text{cm/s}^2)\,k + (75\,\text{cm}^3/\text{s}^2)\,k^3. \tag{13}$$

These results of others are thus plotted at too large a wavenumber because we neglect the wind drift in (13). This is of little consequence as there is little overlap between our data and that of others except in the case of the low wind speed data of Wilson *et al.* (1973) and Gottifredi & Jameson (1970), for which the effect of

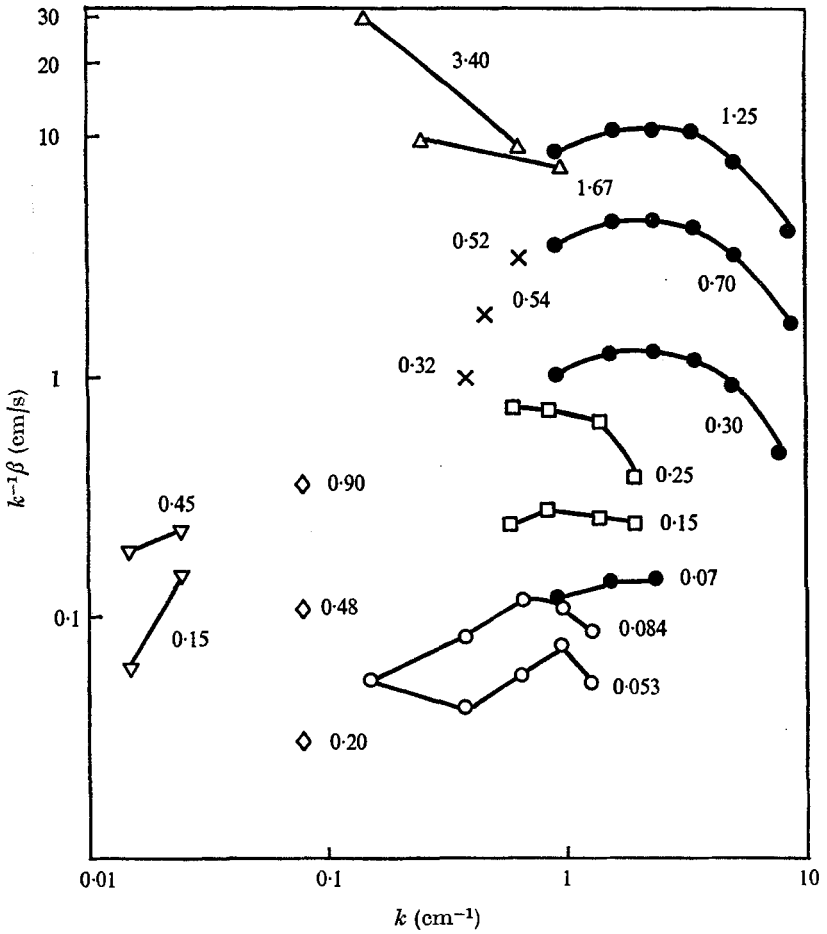

FIGURE 9. Growth rates β divided by k *vs.* k for this work and for the previous growth studies. Friction velocities u_* are given in m/s. △, Sutherland; □, Gottfredi & Jameson; ×, Hidy & Plate; ○, Wilson *et al.*; ▽, Lai & Shemdin; ◇, Hsu & Yu; ●, this work.

the wind drift was small (Keller *et al.* 1974). We believe the agreement between the results of these last-named studies and our results to be quite satisfactory.

Two qualitative observations made during this work should be mentioned. Large-scale tank currents were set up by the wind but we think that they had little effect on the growth rates presented here. These currents in general had an inverse growth rate of minutes or more. Comparisons were made between wind wave growth rates measured immediately (within one minute) after the wind had been blowing at full speed for half an hour and data taken when the tank had been quiescent for at least an hour. The resulting growth rates were identical to within the $\pm 10\,\%$ reproducibility mentioned earlier. The decay of these waves (of 0·7–7 cm wavelength) when the wind is turned off is strongly influenced by the damping rate of the longer-wavelength dominant wave. This, in turn, is complicated by end reflexions. Thus no systematic measurements of decay rates were made.

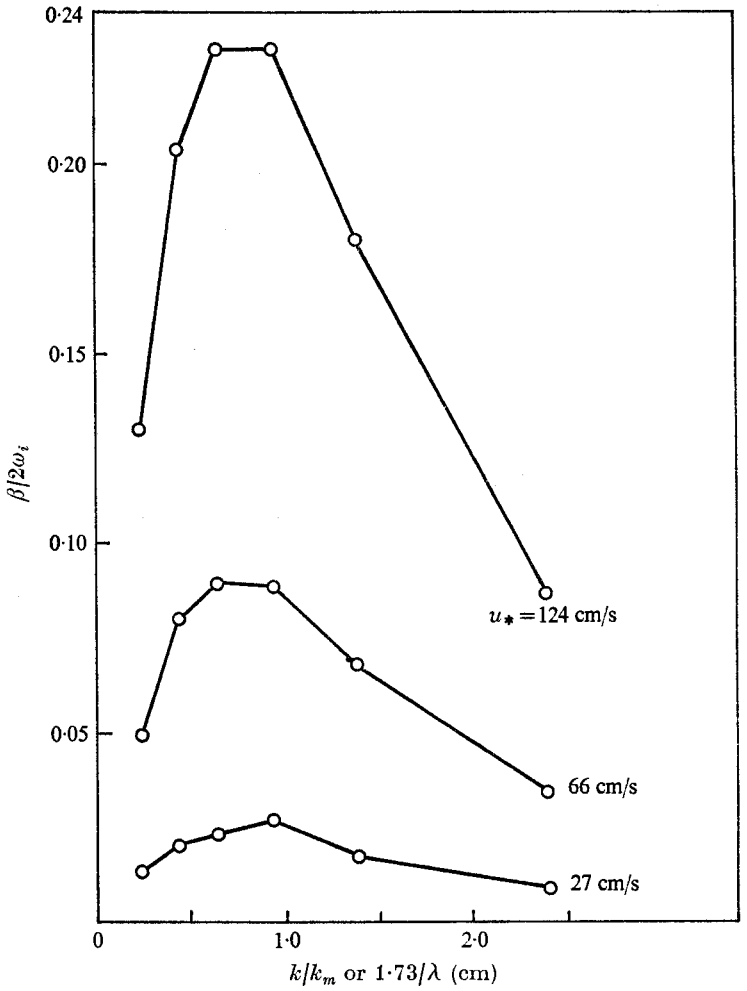

FIGURE 10. $\beta/(2\omega_i)$ *vs.* k normalized by k_m. The amplitude growth rate is $\frac{1}{2}\beta$ and $\omega_i(k)$ is the frequency of an infinitesimal wave of wavenumber k.

5. Discussion

A theoretical interpretation of the results reported here is deferred to a subsequent paper. There are two readily estimated quantities, however, which help to give an intuitive feeling for the magnitude and significance of these growth rates. First, we plot in figure 10 the quantity $\beta/(2\omega_i)$ *vs.* k normalized by k_m for three wind speeds. For each wavenumber, ω_i was obtained from (13). This is an underestimate of the frequency of the waves when viewed from laboratory co-ordinates, because as we view them, the waves are Doppler shifted by mean surface currents towards us. However, $\beta/(2\omega_i)$ is an indication of the strength of the wind–wave interaction. It has a maximum of about 0·2, which indicates tight coupling indeed.

The second quantity is the wind-produced rate of change in wave momentum

per unit surface area. This will be compared with the wind stress estimated from velocity profiles. The momentum density $m(k)$ of a monochromatic irrotational wave can be written as

$$m(k) = \rho k^{-1} V_p(k) S(k), \tag{14}$$

where $V_p(k)$ is the phase velocity, ρ the water density and $S(k)$ the upwind–downwind mean-square slope spectrum. If the energy and momentum input in the steady state are the same as in the initial growth stage then momentum is transferred to the wave of wavenumber k at the rate $\beta m(k)$. The total momentum transfer, which in the steady state must be transferred to the bulk of the fluid or to other waves, corresponds to a stress

$$\tau_w = \int_0^\infty \beta m(k)\, dk. \tag{15}$$

At short fetch $V_p(k)$ is relatively independent of k (Keller *et al.* 1974). Furthermore, referring to figure 10, we approximate β by

$$\beta(k)/k = \beta(k_m)/k_m, \tag{16}$$

so that

$$M \sim \rho V_p(k_m)\,(\beta(k_m)/k_m)\,\overline{S^2}, \tag{17}$$

where $\overline{S^2}$ is the mean-square upwind–downwind slope. At short fetch, the slope of the dominant wave, which makes the bulk of the contribution to τ_w in (15), saturates at $u_* \simeq 50$ cm/s with a value $\overline{S^2} = 0{\cdot}025$ (Keller *et al.* 1974). If we take $\beta_m \sim 10\,\mathrm{s}^{-1}$, $V_p = 30$ cm/s and $u_* = 50$ cm/s the ratio of τ_w to the wind stress $\rho_a u_*^2$ is then

$$\tau/\rho_a u_*^2 \simeq 0{\cdot}75 = O(1). \tag{18}$$

Thus the entire wind stress could be supported by these short gravity–capillary waves alone. An important question is how $\beta(k)/k$ behaves at longer wavelengths. An experiment designed to measure the growth rates of longer waves using bistatic scattering is under way. At any rate, the two comparisons made above, using the growth rates reported here, indicate that short gravity–capillary waves play a significant role in the transfer of momentum from wind to water.

The authors wish to thank W. C. Keller and J. Witting for helpful comments. C. M. Gordon provided the computer program for the least-squares fit.

Appendix A

The wind–wave facility is sketched (not to scale) in figure 1, where important dimensions are given. Wind was generated at the input by a 15 h.p. centrifugal blower 1·5 m in diameter with a calibrated intake shutter. This shutter consisted of two circular, closely spaced plates placed over the blower intake, each with alternate octants removed. Thus it could be abruptly opened to a pre-set final value. The airflow passed through a grate as shown, down a 5 m long uniform wind tunnel and then out over the 13 m long stretch of tap water ending in a downwind beach. The grate served to attenuate unwanted microwave radiation propagating up the wind tunnel. The tank was covered down to the working

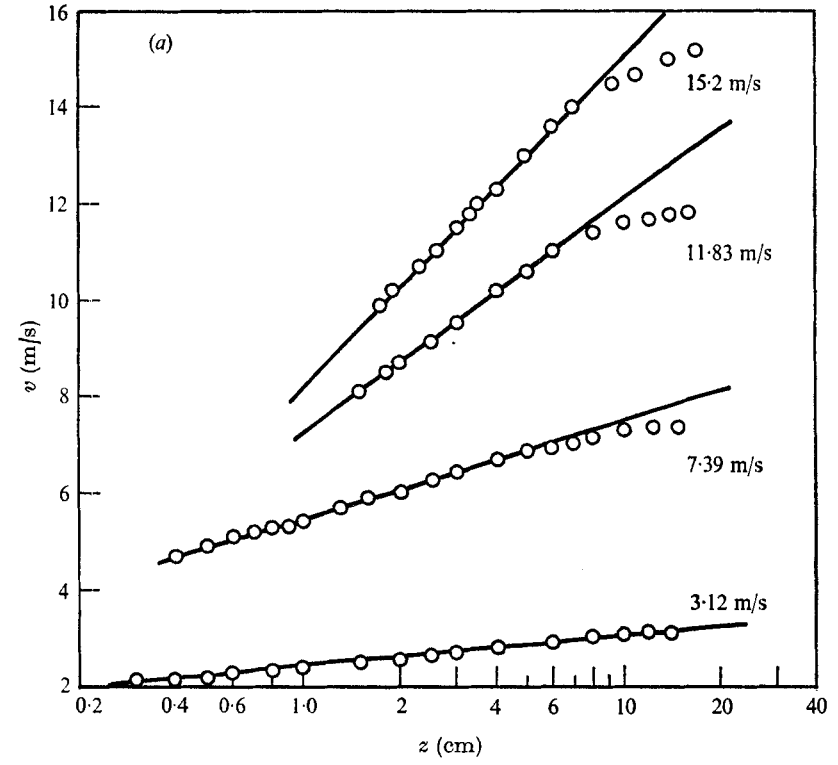

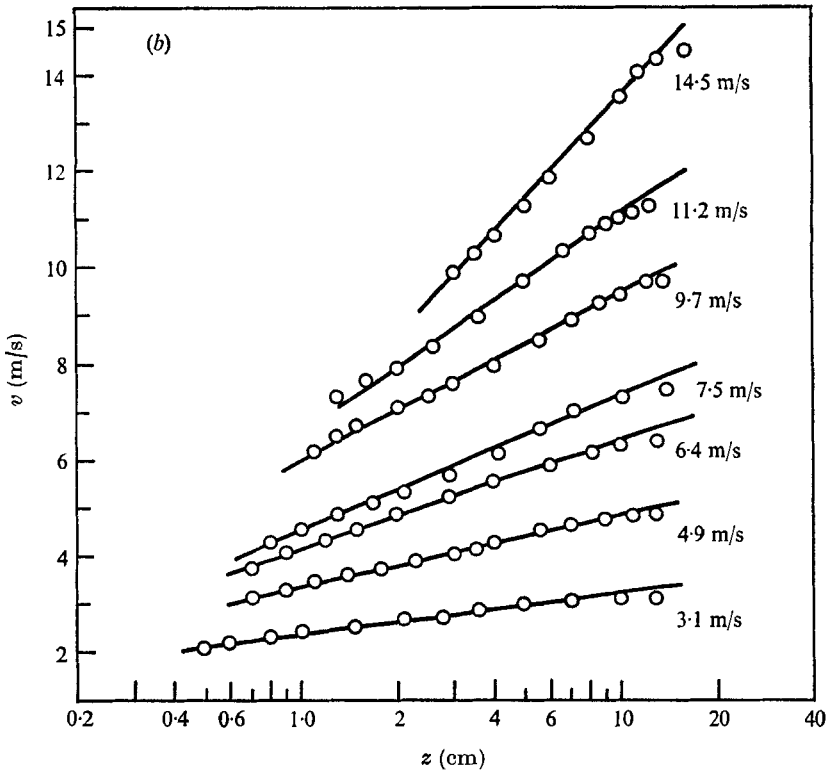

FIGURES 11 (*a*, *b*). For legend see next page.

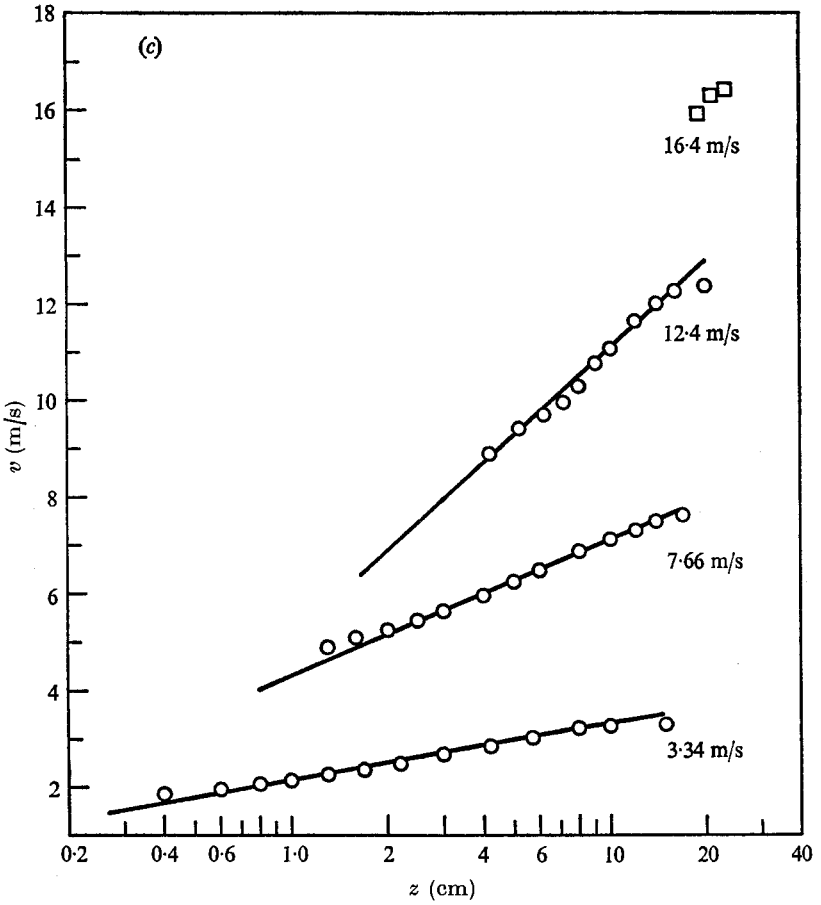

FIGURE 11. Profiles of mean horizontal velocity *vs. z*. (*a*) Fetch = 1·0 m. (*b*) Fetch = 3·0 m. (*c*) Fetch = 8·4 m.

fetches of 1·0, 3·0 or 8·4 m except for the last 1·0 m, which was left uncovered to facilitate the microwave measurements.

The mean wind velocity as a function of vertical position was surveyed for various wind speeds and at several positions in the tank to obtain values of the friction velocity u_* (defined below) and to ensure that there were no gross airflow irregularities. The maximum wind speed was 15 m/s, obtained with a profile with $u_* = 125$ cm/s. A Pitot-static tube 3·2 mm in diameter coupled to an inductive pressure transducer was used for all velocity profiles. This combination was calibrated absolutely using a rotating arm of radius 2 m which moved the Pitot tube through still air. No turbulence corrections were made. To take a profile, the Pitot tube was mechanically scanned vertically with a slidewire rheostat reading out position. The pressure transducer output was plotted directly *vs.* vertical distance using an *x–y* recorder.

A logarithmic profile defined by

$$\bar{v}(z) = (u_*/0{\cdot}41)\ln(z/z_0) \qquad \text{(A 1)}$$

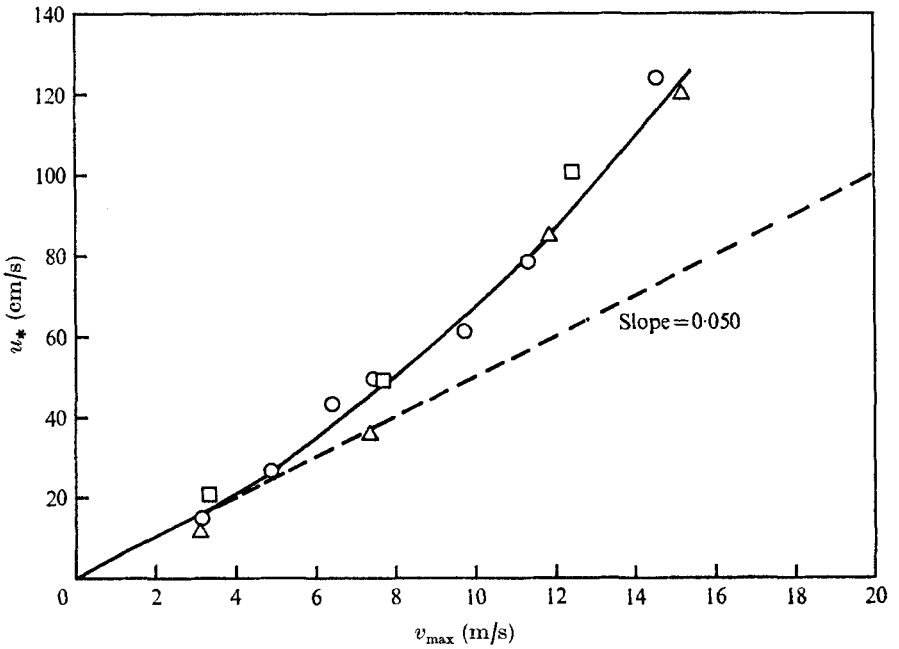

FIGURE 12. Friction velocity u_* *vs.* v_{max} for the profiles of figure 11.
Fetch (m): ○, 1·0; △, 3·0; □, 8·4.

was used to fit the measured profiles and determine u_*. Results from vertical profiles taken along the tank centre-line directly above the centre of the illuminated area are shown in figures 11 (*a*), (*b*) and (*c*) for the three working fetches of 1·0, 3·0 and 8·4 m respectively. The origin of the vertical co-ordinate z was taken at the static water level. The maximum mean velocity plotted in each case is the observed maximum v_{max} in the profile. With z plotted logarithmically, values of u_* are obtained from the slope of the straight lines fitted by eye. The reasonable linear fits indicate fully developed turbulent airflow characterized by a logarithmic profile. An estimate of the statistical error in u_* is 10 %, and perhaps more at low wind speeds, where the Pitot-static tube (a v^2 response instrument) is least sensitive.

For a given shutter setting significant dependence of u_* on fetch was not observed for v_{max} less than about 12 m/s. This can be seen in figure 12, where values of u_* for the three fetches are plotted *vs.* v_{max}. At winds greater than 12 m/s profiles useful for obtaining u_* could not be measured at the longest fetch because the increased wave height and heavy spray prevented the use of the Pitot-static tube near the surface. The linear portion of the dependence of u_* on v_{max} at the lower winds yields a wind stress coefficient

$$C \equiv u_*^2/v_{max}^2 = (2{\cdot}5 \pm 0{\cdot}5) \times 10^{-3}. \qquad \text{(A 2)}$$

The choice of origin for z affects the measured value of u_* since, if all the points on semi-logarithmic plots like those in figure 11 are shifted an equal amount in the z direction, the slope of the plot changes. In making these plots we, as

k (cm^{-1})	c_g (cm/s)	ν [(cm^2/s) $\times 10^{-2}$]
3·02	21·3	1·28
3·08	21·5	1·23
3·41	22·5	1·24
3·69	23·5	1·29
4·23	25·2	1·22
5·00	27·6	1·11
6·44	31·6	1·18
7·62	34·8	1·24
8·67	37·3	1·03
9·40	39·2	1·01

TABLE 3

previously indicated, used the static water level as the origin and thus ignored the set-up. The maximum depression in the mean water level due to the set-up was less than 1·1 cm for all winds and would cause an increase in u_* less than the estimated statistical error of 10 % at winds up to 12 m/s. At the highest wind the set-up would result in a maximum value of u_* of about 145 cm/s rather than 124 cm/s as obtained using the static water level as the origin.

Other checks on the airflow were also made. At the 3·0 m fetch, several vertical profiles were taken at various positions across the tank at the same shutter setting. The resulting u_* variation was within the 10 % error estimate over the central two-thirds of the tank width. At all three fetches, centre-line vertical profiles were also taken just under the tank lid and compared with those 1 m downwind over the illuminated area. The maximum profile velocity v_{max} decreased by approximately 3 % over this distance in the gradually expanding airflow. For the same conditions, however, a statistically significant increase in u_* was observed, with an upper bound of 10 %. Note, however, that the upwind–downwind dimension of the area illuminated by the antenna was always small compared with 1 m.

Appendix B

Surface films of contaminant are an ever-present problem in accurate wave-tank measurements. Several precautions were taken to prevent a significant build-up of such films. A constant trickle of tap water was kept flowing into the tank at the upwind end, and drained off after flowing over the top lip of the beach, as shown in figure 1. Before taking any growth-rate data, the wind was turned on full speed (15 m/s) for at least 20 min, and longer if more than one day had elapsed since the tank had last been used. The shutter 'off' position with the fan running actually left a slight wind, $v_{max} < 0{\cdot}5$ m/s or $u_* < 2$ cm/s. This produced no growing waves, but only a slight surface roughness estimated optically to be less than 0·01 mm in amplitude. This slight wind, however, prevented surface-film build-up.

The viscous damping of mechanical waves with no wind was measured directly, under the clean conditions described above, as a check for surface

contaminants as well as to give an experimental value for the viscous damping correction discussed in §4. Two illuminated slits were suspended at a known separation 2 m above the water surface with a camera midway between them. The images of the slits in the water were broadened by the waves in a readily calculable way. Direct measurements of the attenuation of mechanical waves could thus be made from photographs of the images. The frequency of the mechanical wave was counted accurately, and used to calculate k from (13) in each of several cases. The measured attenuations were equated to give ν. The group velocity c_g was evaluated from (13). The results for ν are given in table 3 together with the values of k and c_g used in each case. The estimated error in ν is 10 %. The values of ν given in table 3 have a mean of 0·0118 cm²/s, which is in reasonable agreement with the value of 0·0114 cm²/s for 15 °C water.† A value of 0·011 cm²/s was used for the correction to the growth-rate data, because the water was slightly warmer for those measurements.

REFERENCES

DUNCAN, J. R., KELLER, W. C. & WRIGHT, J. W. 1974 Fetch and windspeed dependence of Doppler spectra. *Radio Sci.* **9**, 809–819.

GOTTIFREDI, J. C. & JAMESON, G. J. 1970 The growth of short waves on liquid surfaces under the action of a wind. *Proc. Roy. Soc.* A **319**, 373–397.

HASSELMANN, K. 1968 Weak interaction theory of ocean surface waves. In *Basic Developments in Fluid Mechanics*, §5.2. Academic.

HIDY, G. M. & PLATE, E. J. 1966 Wind action on water standing in a laboratory channel. *J. Fluid Mech.* **26**, 651–687.

HSU, E. Y. & YU, H. U. 1970 Laboratory investigation on air–sea interaction. *Proc. 8th Symp. on Naval Hydrodyn.*, paper ARC-179. Office of Naval Research.

KELLER, W. C., LARSON, T. R. & WRIGHT, J. W. 1974 Mean speeds of wind waves at short fetch. *Radio Sci.* **9**, 1091–1100.

LAI, R. J. & SHEMDIN, O. H. 1971 Laboratory investigation of air turbulence above simple water waves. *J. Geophys. Res.* **76**, 7334–7350.

MITSUYASU, H. 1969 On the growth of the spectrum of wind generated waves (II). *Rep. Res. Inst. Appl. Mech., Kyushu University*, vol. 12, no. 59. Fukuoka, Japan.

STEWART, R. H. 1970 Laboratory studies of the velocity field over deep-water waves. *J. Fluid Mech.* **42**, 733–754.

SUTHERLAND, A. J. 1968 Growth of spectral components in a wind-generated wave train. *J. Fluid Mech.* **33**, 545–560.

VALENZUELA, G. R. & LAING, M. B. 1972 Nonlinear energy transfer in gravity–capillary wave spectra, with applications. *J. Fluid Mech.* **54**, 507–520.

WILSON, W. S., BANNER, M. L., FLOWER, R. J., MICHAEL, J. A. & WILSON, D. G. 1973 Wind-induced growth of mechanically generated water waves. *J. Fluid Mech.* **58**, 435–460.

WRIGHT, J. W. 1966 Backscattering from capillary waves with application to sea clutter. *I.E.E.E. Trans. Antennas Propagat.* AP14, 749–754.

WRIGHT, J. W. 1968 A new model for sea clutter. *I.E.E.E. Trans. Antennas Propagat.* AP16, 217–223.

WRIGHT, J. W. & KELLER, W. C. 1971 Doppler spectra in microwave scattering from wind waves. *Phys. Fluids*, **14**, 466–474.

† *Handbook of Chemistry and Physics.* Chemical Rubber Co., Akron, Ohio, 1968.